Applications of Stable Isotopes to Studies of Paleohydrology and Paleoclimatology

Zhengyu Xia and Zicheng Yu

Lehigh University, Bethlehem, PA, USA

1 Fundamentals of Stable Isotope Geochemistry

We first introduce the basics of stable isotope geochemistry and provide readers with the necessary background information in the following sections. For more information on stable isotope geochemistry principles and mechanisms, readers are encouraged to examine the reference books (see Further Reading).

1.1 Basic Concepts

The term *isotope*, derived from Greek, means occupying the same position in the periodic table. Isotopes are variant forms of a particular chemical element that have the same number of protons (atomic number) but differ in the number of neutrons in the atomic mass. Isotopes come in two basic types: radioactive (unstable) and stable. Radioactive isotopes are nuclides that are unstable and spontaneously decay into other new isotopes, whereas stable isotopes are nuclides that do not appear to decay radioactively.

Hydrogen and oxygen have a number of isotopes, including radioactive and stable isotopes. The two stable isotopes of hydrogen, ^{1}H and ^{2}H (also called deuterium and denoted as D), have natural abundances of 99.9885% and 0.0115% in hydrosphere, respectively. The third isotope of hydrogen, ^{3}H (tritium), is unstable with a half-life of 12.23 years. The stable isotopes of oxygen, including ^{16}O, ^{17}O, and ^{18}O, have natural abundances of 99.762%, 0.0379%, and 0.200% in hydrosphere, respectively. Other isotopes of oxygen are radioactive and very short-lived.

In isotope geochemistry, it is a convention to use the atomic abundance ratio of the rare isotope to the major isotope (e.g. $^{18}O/^{16}O$, $^{2}H/^{1}H$) relative to a standard of known isotopic composition to describe the isotopic composition of samples as:

$$\delta\ (\text{in}\ ‰) = \left(\frac{R_x}{R_s} - 1\right) \times 1000$$

where R_x and R_s are the isotopic ratios of the sample and standard, respectively. A positive (negative) δ value means that the measured sample is more (less) enriched in heavy isotope, or heavier (lighter), than the standard. A higher (lower) δ value means that it is more (less) enriched in heavy isotope, or heavier (lighter), than that with lower (higher) δ value. The standard for hydrogen and oxygen isotope measurements of water is the Vienna Standard Mean Ocean Water (VSMOW) from the International Atomic Energy Agency (IAEA), whereas the standard for oxygen isotope measurements of carbonates, such as deep-sea foraminifera, is the Vienna Pee Dee Belemnite (VPDB). The use of international reference standard reduces interlaboratory uncertainties in measuring the absolute ratios of same material on different mass spectrometers. The analytical techniques of mass spectrometry are beyond scope of this article (see Further Reading).

1.2 Isotopic Fractionation

Differences in the atomic mass of isotopes result in slight differences in their physical and chemical properties as isotope effects. This effect is strong for isotopes in low atomic numbers that typically have large relative differences in atomic mass, including $^{18}O/^{16}O$ and $^{2}H/^{1}H$. During physical, chemical, and biological processes or reactions, the relative abundances of different isotopes of the same element change through two phases or two substances. The term *isotopic fractionation* is used to denote the changes in isotopic ratios due to isotope effects. Consequently, different phases or substances attain unique isotopic compositions that are characteristic or indicative to trace their sources and formation environments. Commonly, the magnitude of isotopic

Encyclopedia of Water: Science, Technology, and Society, edited by Patricia A. Maurice.

DOI: 10.1002/9781119300762.wsts0042

fractionation is expressed by fractionation factor (a) between phases (or substances) A and B:

$$\alpha_{A-B}\ (\text{in}\ ‰) = \frac{R_A}{R_B} = \frac{1000 + \delta_A}{1000 + \delta_B}$$

Two kinds of isotope effects, equilibrium and kinetic, can explain most of the isotopic fractionations during various processes on Earth.

1.2.1 Equilibrium Fractionation

Equilibrium isotope effects are the results of atomic effects on bond energy in different phases or substances and are predicted by thermodynamic physics. In terms of qualitative interpretations, heavier molecules have lower zero-point vibrational energy and stronger chemical bonds. Therefore, for a phase change process or isotope exchange reaction, the heavier isotopes preferentially accumulate in the phase or substance with the stiffer bonds or in the higher energy states. For example, as water vapor condenses in clouds, the heavier water isotopes (^{18}O and ^{2}H) become more enriched in the liquid phase because liquid water is denser, whereas the lighter isotopes (^{16}O and ^{1}H) are preferentially remained in the vapor phase. Under such equilibrium fractionation process, the $\delta^{18}O_{liquid}$ or $\delta^{2}H_{liquid}$ values are higher than the $\delta^{18}O_{vapor}$ or $\delta^{2}H_{vapor}$ values, and the fractionation factor $\alpha_{liquid-vapor}$ is larger than 1. Equilibrium fractionation factors are found to be temperature-dependent. It approaches 1 as temperature increases, implying more homogenous isotopic composition between different phases or substances.

The major characteristics of isotopic equilibrium are that the processes or reactions are reversible and that the forward and backward reaction rates are identical. However, this does not mean identical isotopic ratios between two phases or substances. Instead, because of exchange of isotopes, their isotopic ratios are constant over time and in equilibrium condition.

1.2.2 Kinetic Fractionation

Kinetic fractionation arises from fast, incomplete, or irreversible unidirectional processes or reactions. Unlike isotopic equilibrium, the forward and backward reaction rates are not identical. For example, diffusion is one of the kinetic processes. Here, the kinetic energy (E) of ideal gas molecules at a constant temperature is:

$$E = \frac{1}{2} \times mv^2$$

Hence, the differences in atomic mass (m) of a molecule must be compensated for by its velocity (v), that is the heavier molecules have lower velocities and diffuse more slowly during kinetic reactions. For chemical dissociation reactions, heavier molecules have lower zero-point vibrational energy, thus more energy must be taken for dissociation reactions. As a result, kinetic processes tend to make products more depleted in heavy isotopes, or lighter. Such kinetic fractionations are common in biologically mediated reactions, and usually involve isotopic changes in large magnitude.

Evaporation of ocean water is another important kinetic process. Equilibrium fractionation has predicted relatively lower $\delta^{18}O$ or $\delta^{2}H$ values in the vapor phase than the liquid phase. However, the observed isotopic ratio values of marine water vapor are lower than the predicted values. This is due to that evaporation is mostly a unidirectional process as the marine air is unsaturated above oceans and they do not attain isotopic equilibrium. Consequently, the kinetic fractionation further depletes heavy isotopes in the vapor phase and reduces its δ values.

2 Water Isotopes in the Hydrological Cycle

Stable isotopes in water are useful tracers to understand hydrological processes linked to environmental and climatic conditions. A large number and various types of water samples on Earth have been collected for isotopic measurements, including ocean water, meteoric water, surface water, and groundwater. Particularly, the IAEA/World Meteorological Organization (WMO) Global Network of Isotopes in Precipitation (GNIP) program monitored the temporal and spatial variations of isotopic composition in precipitation at global scale for several decades. This observation database helps to understand how water isotopes trace hydrological processes that can be used as a proxy for environmental and climatic parameters. We review the general model of water isotopic distributions and variations in the global hydrological cycle with an emphasis on meteoric water as the basis for understanding its applications in paleohydrology and paleoclimatology.

2.1 Ocean Water

The ocean is the largest water reservoir and water fluxes of evaporation and precipitation over the ocean account for over 90% of the global total water fluxes [1]. In other words, water fluxes over ocean work as the engine of global hydrological cycle. Figure 1a shows the global map of spatial variations of $\delta^{18}O$ values in surface ocean water. The lowest $\delta^{18}O$ values are found in the Arctic and North Pacific Oceans, whereas the highest $\delta^{18}O$ values are found in the Mediterranean Sea, the Red Sea, and other evaporative subtropical oceans. This pattern is similar to surface ocean salinity variations, reflecting evaporative enrichments in ^{18}O in subtropical oceans,

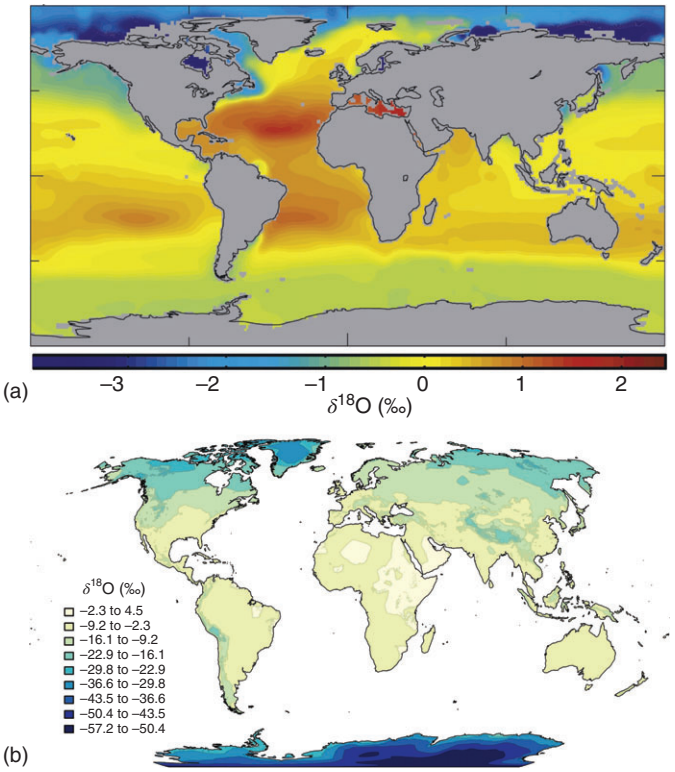

Figure 1 Global map of spatial variations of annual mean δ^{18}O in (a) surface ocean water [2] and (b) precipitation [3]. Both products are interpolated from observation data.

and inputs of ^{18}O-depleted meltwater in high-latitude oceans. The deep ocean water has much more homogeneous δ^{18}O values. The water vapor over ocean, derived from marine evaporation, is depleted in ^{18}O or ^{2}H (having lower δ values) relative to ocean water. A small fraction of evaporated water vapor is advected to continents and converted to meteoric water after condensation and precipitation.

2.2 Meteoric Water

On continents, meteoric water (precipitation) is the ultimate source of water in virtually all terrestrial systems, including lakes, rivers, glaciers, and groundwater. There are large temporal and spatial variations in isotopic composition of precipitation (Figure 1b), which can be satisfyingly explained by condensation processes of air masses approximated by Rayleigh equations.

2.2.1 Rayleigh Distillation

Rayleigh distillation is an important model to account for the changes in isotopic ratios of water vapor and precipitation during condensation processes of air masses. This model assumes partially open equilibrium system for air masses. These equations are:

$$R = R_{\mathrm{i}} \times F^{\alpha-1}$$

$$\delta_{\mathrm{v}} = (\delta_{\mathrm{v,i}} + 1000) \times F^{\alpha-1} - 1000$$

$$\delta_{\mathrm{l}} = (\delta_{\mathrm{v}} + 1000) \times \alpha - 1000$$

where R is the isotopic ratio of water vapor and R_{i} is its initial value. F is the fraction of remaining vapor during continuous condensation, decreasing from 1. δ_{v} is the isotopic composition of water vapor and $\delta_{\mathrm{v,i}}$ is its initial value. δ_{l} is the isotopic composition of liquid (precipitation), and α is the equilibrium fractionation factor between liquid and vapor. The changes in δ_{v} and δ_{l} against F are shown in Figure 2. In this model, the raindrops condensed from the clouds are more enriched in heavy isotope (^{18}O and ^{2}H), making the remaining vapor lighter in isotopic composition, but the falling raindrops would not interact with the vapor after forming precipitation from the cloud system. Therefore, the δ values of vapor become more and more negative during continuous condensation, and the δ values of precipitation also become more negative to track the changes in that of vapor. Furthermore, the equilibrium fractionation factor α is not a constant and tends to increase due to decrease in temperature during the air mass history (Figure 2).

Overall, for a specific air mass, Rayleigh model predicts that the isotopic composition of precipitation is mainly controlled by the extent of rainout and fractionation factor, both of which are related to condensation temperature (see Section 2.2.2). However, it is just a simple approximation for an ideal condensing air mass but does not consider other processes such as moisture recycling from evapotranspiration and mixing

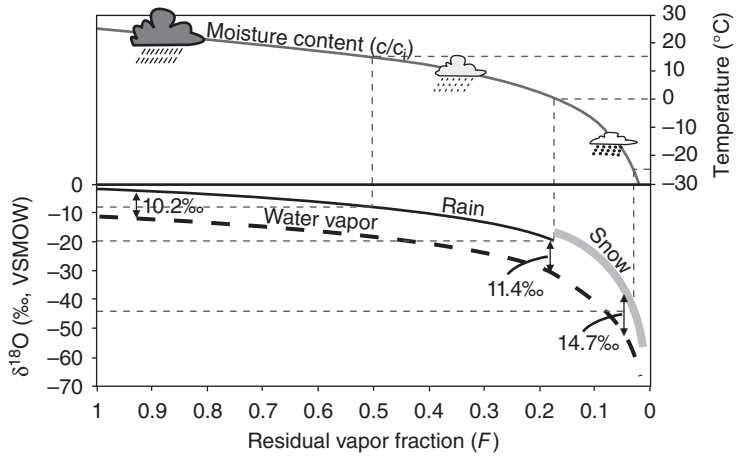

Figure 2 Changes in δ^{18}O of water vapor and precipitation during continuous condensation of an air mass according to the Rayleigh distillation model, starting with δ^{18}O = −11‰ and temperature = 25 °C (Source: Redrawn from [4]). Dashed lines link δ^{18}O of precipitation with temperature of condensation. For example, when an air mass moves to higher latitude or higher altitude, both the isotopic composition of water vapor and precipitation decrease during the proceeding of condensation. In addition, the amplitude of fractionation increases as well because of decreasing temperature. Note that below 0 °C, fractionation between snow and water vapor takes place with higher net fractionation factor due to additional kinetic effect [1].

of different air masses. Other factors influencing the isotopic composition of precipitation include the types of precipitation (rainfall, snow, and fog) and precipitation systems (frontal, orographic, and convective system).

2.2.2 Apparent Effects

Dansgaard [5] examined meteoric water isotope data from around the world and summarized four apparent effects on the temporal and spatial variations of isotopic composition in precipitation (Figure 1b). All these relationships are derived empirically.

2.2.2.1 Latitude effect

Most atmospheric vapor originates from equatorial or subtropical oceans and is carried to high-latitude regions by meridional transports, during which the condensation temperature decreases and the degree of rainout increases. Consequently, isotope δ values of precipitation decrease with increasing latitude, with a spatial slope around −0.6‰ per degree latitude for δ^{18}O [6].

2.2.2.2 Altitude effect

Similar to the latitude effect, adiabatic cooling of air masses during uplift over high-elevation mountains causes strong orographic rainfall, continuous rainout of heavy isotopes, and enhanced fractionation. Therefore, the isotopic composition of precipitation is dependent on altitude, decreasing at an average isotopic lapse rate −2.8‰ per kilometer for δ^{18}O [7]. However, this effect is mostly pronounced on the windward side of mountains.

2.2.2.3 Continental effect

Isotope δ values of precipitation are lower in inland regions than the coastal regions. This phenomenon could also be explained by continuous rainout of heavy isotopes along upstream air masses trajectories and consequently lowered isotope δ values in inland regions.

2.2.2.4 Amount effect

In tropical regions, monthly precipitation isotope δ values are negatively correlated with precipitation amount (Figure 3a) but weakly correlated with air temperature. In addition, this effect is also observed for individual rainstorm events. The precipitation amount effect has been attributed to several factors, including the proceeding rainout of convective clouds, the extent of isotopic exchange, and re-evaporation in descending raindrops [1].

The first three effects mentioned above are all related to air temperature (temperature effect) that can be explained by the Rayleigh model. Figure 3b shows the correlation between amount-weighted precipitation δ^{18}O values and mean annual air temperature from sites around the world; the linear correlation is stronger at mid- and high-latitude regions.

2.2.3 Meteoric Water Line

Craig [8] found the co-variance of δ^{18}O and δ^{2}H values of meteoric water from around the world, which can be described as:

$$\delta^{2}\mathrm{H} = 8 \times \delta^{18}\mathrm{O} + 10$$

which is termed the Global Meteoric Water Line (GMWL). Here, the slope value of 8 is close to the ratio of the equilibrium fractionation factors for two water isotopes. The intercept value of 10 is called the deuterium excess (d-excess). Notably, the GMWL does not intersect with the isotopic composition of "mean" ocean water (δ^{18}O = δ^{2}H = 0 by definition) (Figure 4a), a phenomenon caused by differential kinetic fractionation for two isotopes during the initial evaporation of ocean water.

On the other hand, GNIP program setup monitoring of long-term temporal variations of isotopic composition in precipitation at many locations in the world. For a single site or several sites in a region,

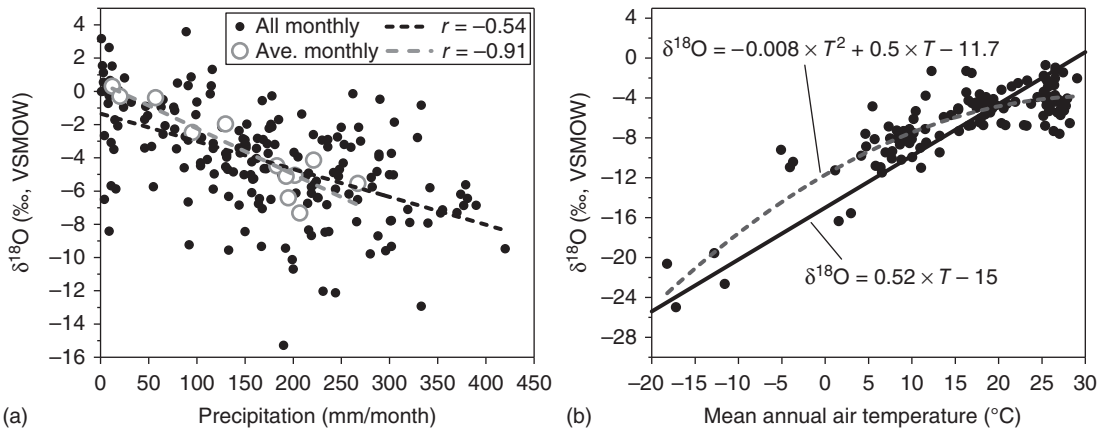

Figure 3 Scatter plots show (a) the amount effect in precipitation from GNIP station in Panama (at 9° N, 1968–1997) for monthly averages (large open grey dots) and all individual months (small filled black dots) of $\delta^{18}O$ values; and (b) the temperature effect in annual weighted mean precipitation $\delta^{18}O$ over period of at least one decade from global GNIP stations (after [6]). The linear relation (slope = 0.52) shown in black line in (b) is based on the data from North Atlantic and European GNIP stations, while the addition of low-latitude station data, influenced by amount effect, tends to make the relation more fitted by second-order polynomial function shown in grey dashed line.

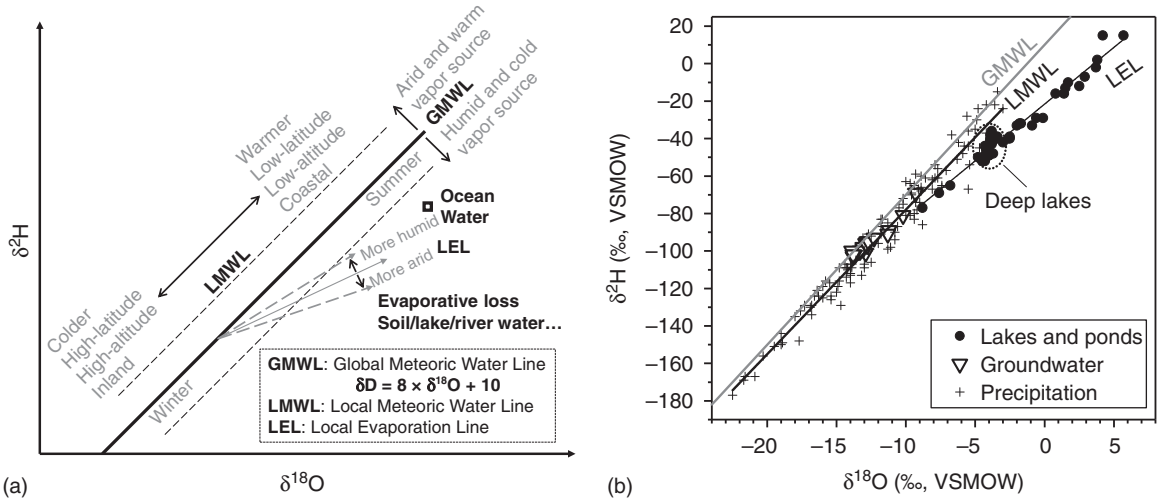

Figure 4 $\delta^{18}O$–$\delta^{2}H$ plots show the relationships among GMWL, LMWL, and LEL. (a) Schematic diagram of isotopic variations in hydrosphere illustrates how hydroclimatic processes affect isotopic composition of water (after [9]). (b) Stable isotopic composition in precipitation, surface water, and groundwater samples collected from Río Gallegos, Argentina, and its surrounding regions (after [10]). The LMWL for this region is regressed as $\delta^{2}H = 7.92 \times \delta^{18}O + 1.22$, divergent from the GMWL. The lake water collected is isotopically evaporated relative to precipitation, with the LEL regressed as $\delta^{2}H = 6.19 \times \delta^{18}O - 22$. The intercept of LMWL and LEL implies the average isotopic composition of meteoric source water that recharges groundwater and lakes.

$\delta^{18}O$ and $\delta^{2}H$ data also show seasonal variations controlled primarily by temperature seasonality in mid- and high-latitude regions. However, the meteoric water line from the local data would deviate somewhat from the worldwide average GMWL with a different slope and y-intercept and is sometimes called the Local Meteoric Water Line (LMWL) (Figure 4a,b). The characteristics of LMWLs provide additional information about the regional hydrological cycle. For example, relatively low slope (5.6) of LMWL is found in Arizona due to partial evaporation of the falling droplets in dry climate [1]. Also, in North America, the LMWL determined by Dansgaard [5] is:

$$\delta^{2}H = 7.95 \times \delta^{18}O + 6.03$$

where the low d-excess relative to GMWL reflects contribution of colder and more humid vapor source from the North Pacific Ocean (Figure 4a). The d-excess parameter of precipitation is found to be an indicator of moisture source regions and conditions [11, 12].

2.3 Surface Water

Meteoric water that is intercepted by tree canopies or reaches the ground will undergo evaporation that enriches ^{18}O and ^{2}H in the residual water, similar to evaporation of ocean water. Consequently, their isotope δ values are higher than that of meteoric source water. On the bi-isotope plot, water isotope data from evaporated waters are plotted below the meteoric water line [8]. For a particular region, these data could be also linearly regressed as the local evaporation line (LEL) (Figure 4a,b). The slope of LEL is less than 8 and is mostly determined by relative humidity of that region, with lower slopes found from more arid regions. It reflects the combination of equilibrium and kinetic fractionations that modify the isotopic composition of water during evaporation [13]. The intercept of LMWL and LEL shows the mean isotopic composition of meteoric source water for the region. One major type of evaporated surface water is lake water in closed basins. The extent of evaporative enrichment or departure relative to its meteoric source water is dependent on the residence time or evaporation/precipitation ratio of that lake. Hence, the effect of evaporative enrichment is significant in large and closed lakes where evaporation predominates. Meteoric water also infiltrates into the ground and become a part of the groundwater in aquifers that are protected from evaporation and keep similar isotopic composition to average precipitation (Figure 4b).

3 Applications in Paleohydrology and Paleoclimatology

The aim of the study of paleohydrology is to reconstruct past changes in water storage and quality, moisture sources, and trajectories and understanding their causes and mechanisms [14]. While the study of paleoclimatology is boarder in aims and scopes and often includes paleohydrology, as past changes in hydrological cycles are tightly coupled with climatic variations. Earth scientists use a variety of proxy data to obtain hydrology and climate information preserved in natural archives. Here, "proxy" is the preserved physical, chemical, or biological indicators of past environments that can substitute for direct meteorological measurements. Proxy archives include marine sediments, ice cores, lake sediments, cave deposits, tree rings, corals, and others. Several independent methods for determining the chronology of these archives have been developed, such as layer counting, radiometric dating, paleomagnetic polarities, and astronomical tuning. After gaining age information, continuous analysis of climate proxies from these archives enables reconstruction of past climate variations from seasonal to orbital and even longer timescales. For more information about the Earth's climate in the past and the techniques of paleoclimate reconstruction, readers should refer to other general sources (see Further Reading).

Water isotopes have been used as proxies in various archives to reconstruct past hydrology and climate changes. However, it is difficult to directly measure the isotopic composition of ancient water samples, with an exception of ice cores. Instead, Earth scientists usually measure the isotopic composition of certain chemical substances, such as oxygen isotope in calcite ($CaCO_3$) and plant cellulose ($C_6H_{10}O_5$), or hydrogen isotopes in lipid biomarkers, e.g. *n*-alkanes (C_nH_{2n+2}). Hydrogen and oxygen atoms of these substances are derived from ambient water during their formation period, thus these substances can be faithful recorders of the isotopic composition of ancient water. However, isotopic fractionations should be considered to infer the paleo water isotopic compositions (Figure 5). As reviewed in Section 2, there are a variety of processes governing water isotopic distributions and variations in hydrological cycles. Therefore, specific interpretations on water isotope proxies in terms of hydrological and climatic indicators in the Earth's past depend on the nature of archives, geographical locations, and timescales. Notably, a necessary assumption is that present isotope proxy-climate relationship is robustly maintained over time, which is supported by climate model simulation results [15]. However, this might not be always a safe premise in isotope-based paleoclimate reconstruction. Hence, multi-proxy approaches that utilize other geological, geochemical, and biological evidence are often applied to constrain the paleoclimate interpretations. In this section, we discuss the applications of stable water isotopes in different archives that address different scientific problems and research questions in paleohydrology and paleoclimatology to highlight both the power and complexity of water isotope proxies. Furthermore, because of the co-variation of two isotopes during isotopic fractionation in hydrological cycles, most studies only use single isotope ($\delta^{18}O$ or $\delta^{2}H$) for paleoclimate reconstruction.

3.1 Deep-Sea Sediments

Oxygen isotope analyses on carbonate shells of fossil foraminifera from deep-sea sediment cores generate continuous records of past global climate variations that have revolutionized climate change science. In many studies, both surface-dwelling (planktonic) and bottom-dwelling (benthic) foraminifera are analyzed, although benthic isotope data are used in most published studies. Through decades of research on numerous cores,

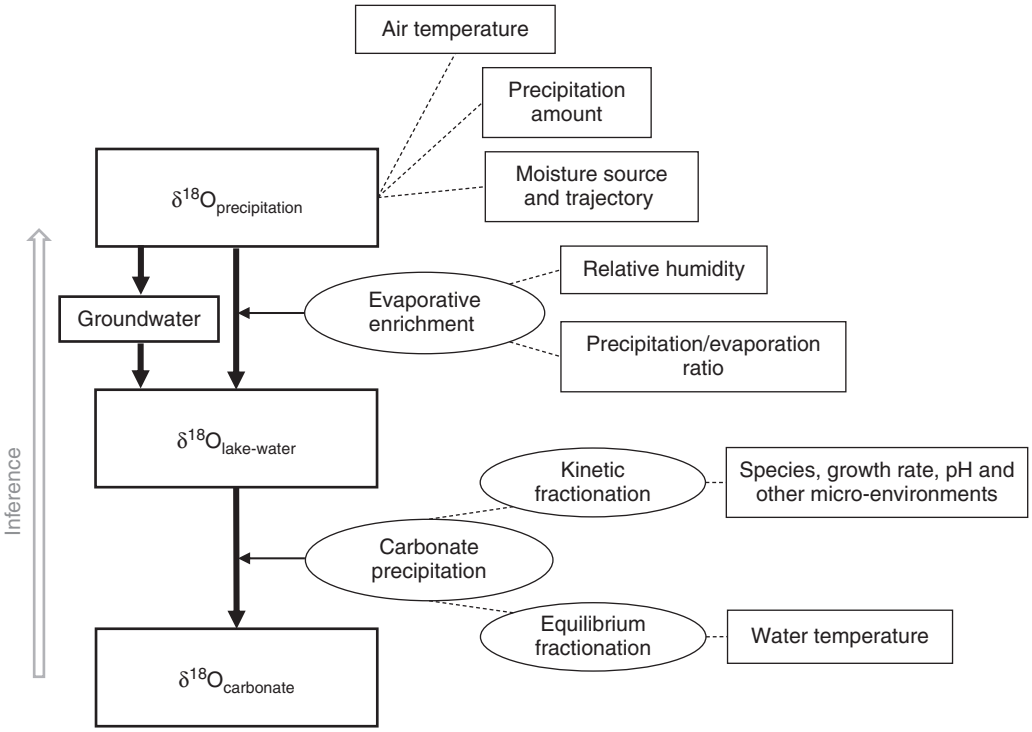

Figure 5 Flowchart shows how the environmental factors control the isotopic values and how paleoclimate information is derived from isotope data, using lake-sediment carbonate as an example. Filled arrows show various processes contributing to $\delta^{18}O_{carbonate}$, where as the hollow arrow shows the direction of inference.

Earth scientists obtain benthic oxygen isotope time series from different ocean basins that show synchronous changes over time. This suggests global oceanographic changes linked to polar ice-sheet dynamics providing clues for understanding climate change mechanisms at tectonic and orbital timescales.

The overall reaction of foraminifera calcite precipitation is:

$$Ca^{2+} + 2HCO_3^- \rightleftharpoons CaCO_3 + CO_2 + H_2O$$

There are two factors controlling foraminifera calcite $\delta^{18}O$ values in deep-sea sediments. First, ocean water $\delta^{18}O$ is the major control on foraminifera $\delta^{18}O$, thus foraminifera $\delta^{18}O$ variations mainly reflect changes in ocean water $\delta^{18}O$ values. Second, equilibrium and kinetic fractionations occur during growth of foraminifera shells that incorporate oxygen atoms from ocean water. Specifically, temperature-dependent equilibrium fractionation factors between marine carbonate species ($CaCO_3, H_2CO_3, HCO_3^-, CO_3^{2-}$) and ocean water have been independently determined as [16]:

$$1000 \times \ln \alpha_{calcite-water} = 18.03 \times \frac{1000}{T} - 32.42$$

Under this expression, calcite $\delta^{18}O$ changes with temperature at about −0.25‰ per °C. On the other hand, kinetic fractionation, known as the "vital effect," is caused by shell growth-rate changes through the life cycle. This effect is minimal for benthic foraminifera in which oxygen isotope equilibrium is maintained.

Lisiecki and Raymo [17] compiled 57 globally distributed deep-sea records to provide a stacked record of oxygen isotopic variations in benthic foraminifera ("LR04") since 5.3 million years ago (Ma). This time series shows a sequence of wave-like isotopic variations that indicate past glacial–interglacial cycles (Figure 6a–c). During glacial periods, foraminifera $\delta^{18}O$ changes to high values because (a) meteoric water/snow with low $\delta^{18}O$ values are stored in expanding polar ice sheets and make ocean water isotopically "heavier," and (b) the fractionation factor between calcite and water increases in cold water. In contrast, during interglacial periods, foraminifera $\delta^{18}O$ switch to low values because (a) ^{18}O-depleted freshwater from melting ice sheets makes ocean water isotopically "lighter," and (b) the fractionation factor between calcite and water decreases when climate warms. Both factors have isotopic effects in the same direction. However, it is a consensus among researchers in this field that the control of ice-sheet size and ocean water $\delta^{18}O$ is dominant over the role of temperature on fractionation factors, while the latter is only important during ice-free greenhouse periods [22]. Therefore, we usually denote the high $\delta^{18}O$ values as cold

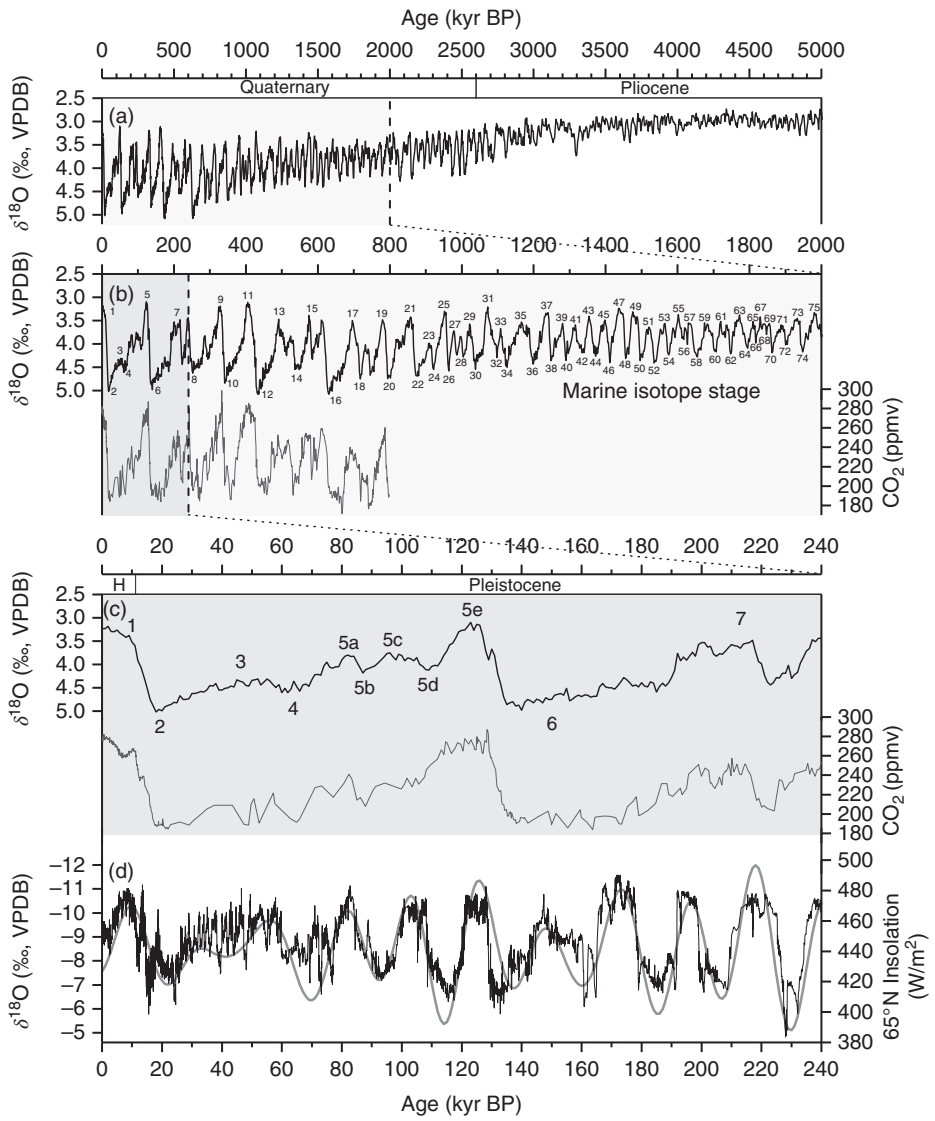

Figure 6 Tectonic- and orbital-scale climate changes reconstructed from foraminifera $\delta^{18}O$ in deep-sea sediments since 5 Ma [17] shown in (a), and close-up since 2 Ma (b) and since 240 ka (c). Also shown in (b) and (c) are the Marine Isotope Stage (MIS) numbers and the atmospheric CO_2 concentration record from Antarctic ice cores [18]. In (c), MIS5 is divided into five substages, including the last interglacial 5e, and "H" means the Holocene Epoch. (d) The composite cave $\delta^{18}O$ record of EASM variations [19, 20] and 65° N summer insolation [21] shows that EASM is forced by precession cycle. Note that all *y*-scales of $\delta^{18}O$ are in reverse.

glacial periods and the low $\delta^{18}O$ values as warm interglacial periods. The alternating glacial and interglacial periods are marked by even numbers and odd numbers of the Marine Isotope Stages (MIS), respectively.

The LR04 curve shows long-term increase in benthic foraminifera $\delta^{18}O$ values responding to long-term Cenozoic (since 65 Ma) cooling trend from greenhouse to icehouse climates [22]. Furthermore, the amplitude of benthic $\delta^{18}O$ variability increases considerably at around 2.7 Ma (the start of the Quaternary Period or Pleistocene Epoch) (Figure 6a); this transition marked the onset of major Northern Hemisphere glaciation and subsequent periodically waning and waxing of ice sheets [23]. The second amplification of benthic $\delta^{18}O$ variability occurred at the mid-Pleistocene around 0.9 Ma. This transition is not only reflected in the amplitude of variability, but also in the shift of dominant periodicity and the shape of glacial–interglacial cycles (Figure 6b). Before 0.9 Ma, benthic $\delta^{18}O$ variability across glacial–interglacial cycles is symmetrical and centered on a periodicity of 41-thousand-year (kyr). After 0.9 Ma, however, $\delta^{18}O$ variability is characterized by saw-toothed shape with abrupt transitions into interglacials but slow-paced transition into glacial maxima, as well as a dominant periodicity of 100-kyr. Earth's climate today is on the start of slowly natural cooling trend from interglacial maximum (Figure 6c), but it tends to be reversed due to anthropogenic global warming since the industrial era. Overall, taking LR04 as an example, deep-sea benthic foraminifera $\delta^{18}O$ records document the dynamics of oceanographic and ice-sheet changes in the past that are forced by cyclic variations in the Earth's orbital parameters [24].

3.2 Ice Cores

Glacier ices are formed through compression of accumulated snows under their own weight over time. Continental ice sheet drilling projects on the Greenland and Antarctica retrieved kilometer-long ice cores, while their ages could be directly determined by counting the annual layers or indirectly using ice flow models. Physical and chemical property analyses on ice core samples yield continuous proxy records characterizing past climate and atmospheric history over hundreds of thousand years. For example, ancient air bubbles trapped in the deep ices directly inform us past atmospheric greenhouse gas concentrations [18, 25]. In this subsection, we focus on the use of water isotopes in ice cores as local air temperature proxy that document continental climate changes of two hemispheres during the late Pleistocene, particularly the millennial-scale rapid climate oscillations that are often not fully resolved in deep-sea sediments.

Ice cores store ancient precipitation. Therefore, their $\delta^{18}O$ and $\delta^{2}H$ variations directly reflect changes of isotopic composition in snowfall over time. Also, this allows the application of d-excess as a moisture source tracer in ice-core studies [26, 27]. In polar regions, air temperature exerts the dominant control on the isotopic composition of meteoric water (Figure 3b). For example, isotope δ values of snowfall in warmer ice sheet margin are higher than that in colder and higher-elevation ice sheet dome. In addition, isotope δ values of summer snowfall are higher than that of winter snowfall. However, the slope of the temperature-water isotope relations tends to be inconsistent between spatial and temporal scales [28]. Nevertheless, isotopic composition of ice cores is the direct proxy for local air temperature.

A few deep Greenland ice cores have been drilled by international communities that retrieve climate records covering full last glacial period until 105 thousand years ago (ka). An ice core drilled for the North Greenland Ice Core Project (NGRIP) is dated to the last interglacial until 123 ka [29]. One of the key features of the Greenland $\delta^{18}O$ record is the millennial-scale fluctuations at a magnitude of 4‰ that occurred 25 times during the last glacial period (Figure 7c). These rapid climate changes are termed as the Dansgaard–Oeschger

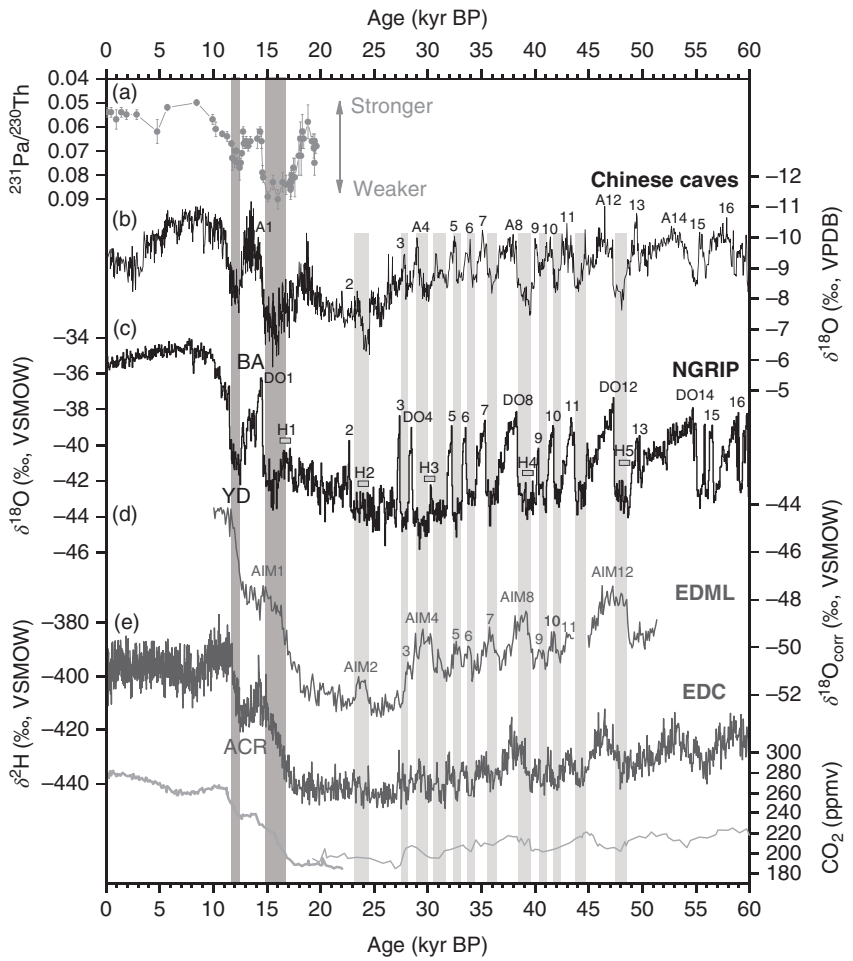

Figure 7 Millennial-scale climate changes and the bipolar seesaw pattern during the last 60 kyr. (a) $^{231}Pa/^{230}Th$ record from a deep-sea core in the western subtropical Atlantic Ocean as a proxy for AMOC strength [30], showing weaker AMOC during H1 and YD; (b) the composite cave $\delta^{18}O$ record from China as a proxy for EASM strength [19, 20], with the numbers marking Chinese interstadials (A1–A16); (c) the NGRIP ice-core $\delta^{18}O$ record as a proxy for Greenland air temperature [29], with the numbers marking DO and H events; (d) the European Project for Ice Coring in Antarctica (EPICA) Dronning Maud Land (EDML) ice-core $\delta^{18}O$ record as a proxy for Antarctic air temperature for the Atlantic sector, with the numbers marking AIM [31]; (e) the same with (d) but is ice-core $\delta^{2}H$ record from EPICA-Dome C (EDC) located in the Indo-Pacific sector of Antarctica [32]; (f) atmospheric CO_2 concentration record from Antarctic ice-core [25, 33]. The period of LGM, BA, YD, and ACR are denoted. The grey bars indicate the intervals of millennial-scale Greenland cooling and EASM strength reductions concurrent with Antarctic warming, a phenomenon known as the bipolar seesaw, despite there are few misfits due to uncertainties in ages. Note that the *y*-scales in (a) and (b) are in reverse.

(DO) oscillations, with interstadial warm events (DO events) numbered. In contrast, the present interglacial (the Holocene Epoch) is markedly stable. Furthermore, the transition from the Last Glacial Maximum (LGM, ~21 ka) to the Holocene, referred as the last deglaciation or ice age termination, is also associated with several millennial-scale climate oscillations, including the Heinrich event 1 (H1), the Bølling–Allerød (BA) warming, and the Younger Dryas (YD) cooling (Figure 7c). Particularly, the Heinrich events indicate layers of lithic fragments in deep-sea sediments of the North Atlantic that were discharged from melting icebergs during the deglacial warming. These climate oscillations during the last deglaciation are representative for other rapid climate events recorded in Greenland ice cores and hence have been extensively investigated.

These millennial-scale climate oscillations are also observed in Antarctic ice cores (Figure 7d,e) [32]. By tuning the chronology between Greenland and Antarctic ice core records using methane synchronization, we can directly compare the timing and duration of these rapid climate changes at two polar regions to investigate global climate teleconnections. At the onset of the last deglaciation, climate warming was rapid in Antarctica and paralleled with CO_2 increase (Figure 7f), to a peak value at 14.7 ka, termed as the Antarctic Isotope Maxima 1 (AIM1), whereas climate warming in Greenland was relatively slow and punctuated by H1 cold condition at 16.8–14.7 ka. Subsequently, Antarctica experienced the Antarctic Cold Reversal (ACR) at 14.7–12.7 ka, a cold period when Greenland experienced BA warming (DO1). The end of ACR at 12.7 ka was followed by Antarctic warming continuing to the warmest period during the early Holocene, while over Greenland there was the YD cooling at 12.9–11.7 ka. Overall, Antarctic cooling/warming is associated with Greenland warming/cooling. This phenomenon is known as the bipolar seesaw caused by heat transport through the Atlantic Meridional Overturning Circulation (AMOC) between two hemispheres. During the last deglaciation, freshwater injection during iceberg discharge decreased the surface ocean salinity and created a colder and fresher water lid over the North Atlantic that reduced deep-water formation and shut down or slowed down the AMOC, such as during H1 and YD (Figure 7a). The failure of AMOC suppressed heat transport through surface flow from the South Atlantic to North Atlantic and resulted in the Greenland cooling. The heat remained in the southern hemisphere resulted in the Antarctic warming. In contrast, the recovery of AMOC led to reverse processes that warmed Greenland but cooled Antarctica. The mechanism of bipolar seesaw is thought to hold consistently for other series of rapid climate change events in Antarctica and Greenland. For example, the amplitude of the AIMs is found to be linearly dependent on the duration of the Greenland cooling since the MIS3 [31]. Overall, ice core studies from two poles provide insights into the processes of millennial-scale climate changes and ocean–atmosphere teleconnection mechanisms.

3.3 Lake Sediments

Lake water and other surface water consist of less than 0.01% in global water budget, but they are important freshwater resources for human lives and agricultural, domestic, and industrial uses. Therefore, documenting past land water resource availability is critical for understanding the patterns of floods and droughts and their relationships with climate dynamics. Lake basins are ubiquitous continental archives around the globe and have been targeted of paleohydrology and paleoclimate studies for decades. There are many methods to reconstruct past variations in lake-level, water temperature, and chemistry using radiocarbon-dated lake-sediment cores, whereas geomorphological remains and seismic surveys provide additional evidence. Unlike the deep-sea and ice core records that integrate large-scale oceanic and atmospheric changes, lacustrine records tend to reflect more regional-scale climate variability and dynamics.

Lake basins directly receive rainfall and snowfall, thus isotopic composition of lake water reflects that of mean annual precipitation in small-to-medium and hydrologically open lakes. For large or hydrologically closed lakes, lake water has long residence times of decades or centuries. Consequently, isotopic composition of lake water is modified by evaporative enrichment in heavy isotopes and their isotope δ values are higher than the mean annual precipitation isotope δ values. As a result, the size and hydrology of lake matter in the paleoclimatic interpretation from lacustrine isotope records [34].

Lacustrine sediments are typically composed of carbonates, organic matter, and silicates. Among them, biogenic or authigenic carbonates are commonly used for oxygen isotope analysis. Like the deep-sea foraminifera, factors controlling lacustrine carbonate $\delta^{18}O$ include the lake water $\delta^{18}O$ and the fractionation factor (Figure 5). Equilibrium fractionation between precipitated carbonate and lake water is also dependent on lake water temperature. The effect of kinetic fractionation is minimal for authigenic carbonates or could be minimized by modern calibration studies that quantify these systematic offsets for other biogenic carbonates [34]. For lake-sediment cores that do not contain lacustrine carbonates, compound-specific hydrogen isotope analysis on lipid compounds sourced from aquatic and terrestrial plants have been used to derive isotope records comparable to carbonate oxygen isotope analysis [35].

The mechanism of hydrogen isotope fractionation processes for plant lipids were investigated, and their fractionation factors have been quantified in several studies [36]. Silica shells of diatom algae ($SiO_2 \cdot nH_2O$) [37] and cellulose of aquatic moss macrofossils [38] are also among the targets for isotope analysis if lake carbonates are absent.

To quantitatively interpret lacustrine isotope records for climate change, it is necessary to diagnose these two factors (lake water $\delta^{18}O$ and the fractionation factor) controlling down-core isotopic variations. Notably, in mid- and high-latitude regions, the temperature effects on precipitation $\delta^{18}O$ and on fractionation factor result in changes in lacustrine carbonate $\delta^{18}O$ in opposite directions. However, the positive effect of meteoric water $\delta^{18}O$ (around +0.6‰ per °C) [39] is more important than the negative effect of fractionation factor (−0.25‰ per °C). Considering both effects, a net carbonate $\delta^{18}O$-temperature gradient of +0.35‰ per °C is a robust approximation to estimate paleotemperature changes in mid- and high-latitude regions. A lake ostracod carbonate $\delta^{18}O$ record from southern Germany shows synchronous air temperature changes with Greenland ice core record from 15.5 to 5.0 ka [40], suggesting climate teleconnection within the North Atlantic. In tropical regions, the "amount effect" of isotopic composition in precipitation is used in most studies. More negative isotope δ values reflect more precipitation amount and vice versa. In addition, higher precipitation amount and wetter climate reduce evaporative enrichment in heavy isotopes and further lower lake water isotope δ values. For example, biomarker δ^2H record from Lake Tanganyika in tropical southeast Africa document abrupt onset and termination of early Holocene humid period [41]. Overall, in tropical regions, lacustrine isotope records primarily provide insights into paleohydrological changes. Despite this, we highlight that many other factors could have influence on lacustrine isotope data and simple proxy interpretation for single meteorological factor is not always justified (Figure 5). Particularly, differences in moisture sources and trajectories, as well as atmospheric circulation patterns, are important in past climate states. On the other hand, lacustrine isotope data from large and hydrologically closed lakes primarily document changes in precipitation/evaporation balance [34]. Therefore, multi-proxy methods are often applied in paleohydrology and paleoclimate reconstructions from lacustrine sediments. For example, multi-proxy reconstruction from Lake Bosumtwi, Ghana, document long-term multi-decadal Sahel drought patterns (Figure 8) [42]. Furthermore, recent methodological innovations were made toward more quantitative interpretations on lacustrine water isotope records. One new method is to combine carbonate $\delta^{18}O$ records from open and closed lakes in the same region to deconvolve the signal of precipitation/evaporation balance from the changes in precipitation $\delta^{18}O$, which could provide more robust estimations on past moisture availability [43]. Another new method is to combine carbonate $\delta^{18}O$ data and biomarker δ^2H data to reconstruct the changes in the extent of evaporative enrichment of lake water and precipitation δ values [44].

3.4 Speleothems

Speleothems are carbonate mineral deposits formed from dripping water in underground karst caves. The drip-water in caves, originally sourced from above-cave meteoric water, has high concentrations of calcium and bicarbonate as they react with CO_2 and dissolve calcium carbonate bedrock during infiltration through soils and carbonate bedrock. The low CO_2 concentration environment in caves drives precipitation of calcite

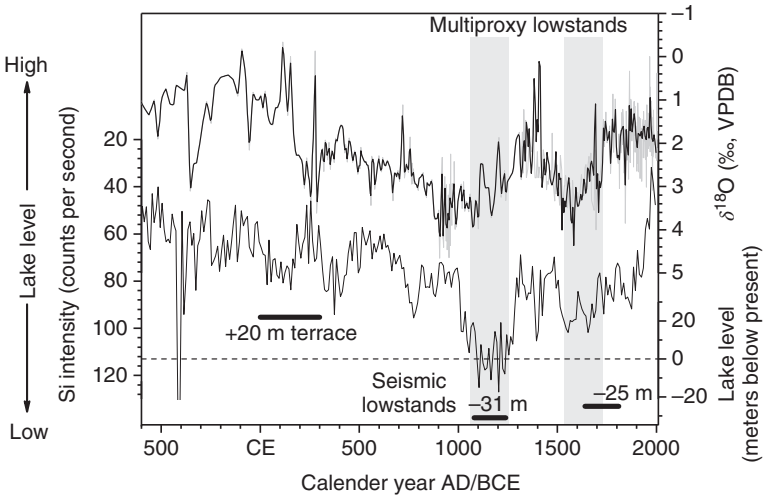

Figure 8 Paleohydrological evolution of Lake Bosumtwi revealed by multi-proxy data, including carbonate $\delta^{18}O$ (raw data in thin grey lines and 5-year average in thick black lines), silicon (Si) intensity generated by X-ray fluorescence (XRF) that indicates terrigenous material inputs (in reverse scale), and lake-level estimates based on lake terraces and seismic profile. (Source: Redrawn from [42]). The grey bars indicate the periods of multi-proxy lowstands and droughts during the last millennium. Here higher carbonate $\delta^{18}O$ values suggest more evaporative condition in period of drier climate.

carbonate from drip-water. Thus, speleothems are like other terrestrial archives for documenting past continental climate during which they grew. Of advantage for speleothem archives for developing paleoclimate records is they can be precisely dated by Uranium-series methods. In addition, some speleothems contain visible annual growth bands, thus precise ages could be determined by layer counting and records could be resolved in seasonal or annual resolutions. However, because deposition of speleothems relies on sufficient drip-water supply and sometimes speleothems contain growth hiatus (a pause of speleothem deposition often due to dry condition), usually a set number of speleothem columns are needed to provide continuous records from a region.

The controlling factor on speleothem calcite $\delta^{18}O$ values is similar to lacustrine carbonate, but some additional cave-specific processes influence drip-water $\delta^{18}O$ values [45]. First, soil water might experience evaporative enrichment in ^{18}O before infiltrating downward, especially in arid regions. Second, the timing and amount of soil water recharge to fractures and joints of carbonate bedrocks controls drip-water $\delta^{18}O$ values. For example, drip-water of caves in Nevada show low $\delta^{18}O$ values comparable with winter snowfall $\delta^{18}O$ values [46]. In this case, speleothem calcite $\delta^{18}O$ records should be interpreted for winter-season signal. Third, the transit-times of soil water into caves can be long and isotopic composition of drip-water might have delayed responses to climate variability. This effect is important for high-resolution climate studies.

Interest in speleothem-based paleoclimate reconstruction has increased rapidly in the recent decades due to the ability to produce high resolution and reliable chronologies. Major high-profile studies on speleothem $\delta^{18}O$ records from southeastern Asia show that they document orbital, millennial, and centennial-scale variability in monsoon intensity and rainfall amount [19, 20, 47]. Figure 6d shows the composite $\delta^{18}O$ cave record of East Asian Summer Monsoon (EASM) since the last two interglacials reconstructed from multiple Chinese speleothems. There are several important findings from these records. First, the EASM fluctuations broadly follow orbitally induced Northern Hemisphere summer insolation with a dominant variance of 23-kyr precession cycle (Figure 6d); higher summer insolation induces stronger EASM. Second, millennial-scale intensifications in EASM punctuate orbital-scale variability, and they are synchronous with DO warming events recorded in Greenland ice cores during the last glacial (Figure 7b,c) [48]. Third, centennial-scale reductions in EASM are linked with North Atlantic Bond cold events and low solar activity [47]. These series of in-phase correlations on various timescales suggest hemisphere-wide climate teleconnections between high- and low-latitude regions during past climate changes. On the other hand, monsoon rainfall from EASM is critically important for this populated region, whereas droughts and floods associated with EASM variability are major natural hazards that influence agriculture and human societies. Overall, these speleothem $\delta^{18}O$ records contribute to our understanding on past EASM variability and its teleconnection mechanisms.

However, there are controversies on the interpretation of speleothem $\delta^{18}O$ as a proxy for monsoon intensity. One viewpoint is that higher proportion of summer monsoon rainfall (low $\delta^{18}O$ values) relative to annual total rainfall decreases the $\delta^{18}O$ signals in speleothem records [48]. It implies that lower speleothem $\delta^{18}O$ values reflect higher precipitation amount at cave site during stronger monsoon periods. Another viewpoint is that an increase of upstream rainfall from air masses destined for cave sites decreases the $\delta^{18}O$ signals in speleothem records [49]. It is based on the Rayleigh fractionation of water vapor originating from oceans and implies that lower speleothem $\delta^{18}O$ values reflect lower precipitation $\delta^{18}O$ values, rather than precipitation amount. Recent advances in the analytic techniques of speleothem calcite isotope provide new insights into these controversies. For example, ion microprobe now is capable of high-precision and accurate *in-situ* $\delta^{18}O$ measurements in 10-mm-diameter spots in speleothem calcite, offering opportunities to reconstruct seasonal variability of calcite $\delta^{18}O$. One study using this technique on a Chinese cave suggested that both viewpoints are supported and they are compatible [50].

3.5 Biological Archives

Some living organisms have annual growth layers that serve as biological archives of seasonal or interannual signals of their living environments. Tree rings and corals are typical examples of this category.

3.5.1 Tree Rings

Annual tree rings are recorders of their growing history during their lifespan. In addition to tree-ring widths and densities, stable isotopes of tree-ring cellulose can also be used as a proxy for environmental conditions. The processes of tree-ring cellulose synthesis and isotopic fractionations associated with them are important for understanding the controlling factors of tree-ring isotopes [51]. The moisture source for trees is soil water that is taken-up by tree roots through xylem and transported to leaves for photosynthesis. Then photosynthesized sugars are transported down to trunk for cellulose synthesis, during which there are isotopic exchanges with xylem (source) water. Therefore, oxygen isotopic composition

of tree-ring cellulose is primarily determined by the isotopic composition of precipitation and the extent of evaporative enrichment in ^{18}O in soils and leaf stomata. Correlation analyses between tree-ring cellulose isotope values and meteorological parameters during instrumental period are used to calibrate their empirical relationships. For example, it was found that tree-ring cellulose $\delta^{18}O$ and total precipitation are negatively correlated during twentieth century in northern Pakistan, thus tree-ring isotope data are used to reconstruct past rainfall variability prior to instrumental period in this region [52]. Furthermore, because tree-ring records are resolved in seasonal and interannual scales, they are useful for studying high-frequency climate variability. Another study showed that low $\delta^{18}O$ spikes in tree-ring cellulose records from the southeastern United States are indicators of past tropical cyclone activity over the last 220 years [53].

3.5.2 Corals

Corals typically live as colonies in warm and productive shallow tropical oceans and form brightly colored mounds. Their growth is very sensitive to surface ocean water temperature, clarity, and nutrient availability. Coral skeleton aragonite ($CaCO_3$ with different crystal structure from calcite) shells add annual bands during growth. High-resolution isotope analysis on these layers, along with Uranium-series chronology, build time series of tropical sea surface temperature (SST) and salinity, both of which are related to the El Niño-Southern Oscillation (ENSO). The ENSO is an interannual climate variability related to tropical ocean–atmosphere dynamics that influences global climate through teleconnections. During warm phase known as El Niño, tropical eastern Pacific Ocean is warmer than normal; during cold phase as known as La Niña, tropical eastern Pacific Ocean is colder than normal. A study showed that $\delta^{18}O$ variations of living coral bandings are negatively correlated with SST anomalies in central tropical oceans (Figure 9) [54]. Warmer and wetter conditions during El Niño years result in lower aragonite $\delta^{18}O$ by decreasing the fractionation factor and surface ocean water $\delta^{18}O$ values and vice versa for La Niña years. Taking this relationship to the analyses of fossil corals, it is effective to detect the past changes in ENSO variances. Analyses on fossil corals spanning the past 7000 years showed that the ENSO is very dynamic and there is no apparent link between ENSO variance and climate mean states [54, 55]. These studies provide insights into future ENSO regime under anthropogenic warming.

3.6 Other Climate Archives

Many other natural archives have been developed for stable isotope analysis that enables paleohydrology and paleoclimate reconstructions. Peat deposits in wetlands accumulate partially decayed vegetation materials in anoxic conditions that are suitable for organic matter isotope analysis. For example, a 14.5-kyr organic matter $\delta^{18}O$ record from Alaskan peat documents variations in temperature and atmospheric circulation patterns [56]. Other peat studies use extracted cellulose $\delta^{18}O$ or lipid biomarkers $\delta^{2}H$ for paleoclimate interpretations [57, 58].

Furthermore, soil carbonates formed under a net water deficit and preserved in paleosols can serve us another archive of continental climate history [59, 60], particularly for pre-Quaternary paleoclimate reconstructions. The oxygen isotopic composition of paleosol carbonates is controlled by the isotopic composition of ancient meteoric water and the temperature of formation. Large-magnitude shifts in paleosol carbonate $\delta^{18}O$ relative to today reflect changes in elevations, topography, atmospheric circulation patterns, and air temperature. Therefore, stable isotopes of paleosol carbonates are important tool to unravel landscape evolution at tectonic scales [61]. Although uncertainties are associated with multiple controlling factors on carbonate $\delta^{18}O$ and diagenesis processes are inevitable for these old-aged carbonates minerals, recent advances in analytical techniques offer more constraints on the isotope studies of paleosol carbonates [61, 62].

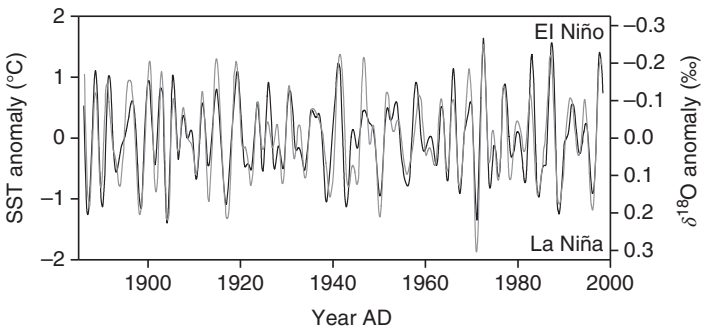

Figure 9 Palmyra modern coral record of $\delta^{18}O$ anomalies (grey line, bandpass filtered in 2–7 years and in reverse scale) from central tropical Pacific Ocean plotted with Niño3.4 sea surface temperature (SST, black line) anomalies during the twentieth century. (Source: Redrawn from [54]). This shows coral $\delta^{18}O$ is a sensitive recorder of SST variations related to the ENSO.

4 Multi-Proxy Approach to Constrain Isotope-Based Paleo Interpretations

Multiple environmental parameters influence the isotopic composition of lake carbonate as shown in Figure 5. The general flowchart is also applicable to other terrestrial archives, such as speleothem and paleosols. In order to interpret isotopic variations as reflecting certain aspects of the hydrological cycle or climatic changes, it is necessary to understand the dominant factor(s) controlling the water isotopic variations in the context of paleoclimate reconstruction. It does not mean only one or two factors influence the isotopic composition of carbonate, but the major drivers of changes that predominate over other factors. One way to determine the controlling factors on isotopic variations is to investigate the modern processes of isotopic response to spatial climate gradients or temporal climate variability. However, the proxy-climate relationships inferred from modern process studies might be nonstationary and invalid to account for the isotopic variations over longer timescales. Another desirable way is to utilize other physical, chemical, and biological proxy data from the same sites to constrain the interpretations from isotopic variations.

In the studies of deep-sea foraminifera, it is widely accepted that benthic foraminifera shell $\delta^{18}O$ primarily reflects the ice volume rather than deep ocean temperature during Quaternary glacial–interglacial cycles (see Section 3.1). However, this qualitative interpretation of isotope data impedes further understanding of the interplay between ice-sheet growth and global climate patterns. Studies showed that the signal of ice volume changes could be isolated from foraminifera $\delta^{18}O$ by combining independent deep-ocean water temperature proxy data [63], such as the ratio of magnesium to calcium concentration (Mg/Ca) of the benthic foraminifera that are found to be positively correlated with water temperature. By removing the influence of deep ocean temperature on benthic foraminifera $\delta^{18}O$, the residual $\delta^{18}O$ reflects changes in ice-volume history (Figure 10). This shows the usefulness of multi-proxy in deep-sea sediment studies.

Multi-proxy approaches are particularly successful in lake-sediment studies that contain integrated information from local lake dynamics and regional catchment history [65]. One example of multi-proxy application is the study of Crawford Lake in southern Ontario, Canada (Figure 11) [66, 67]. Carbonate $\delta^{18}O$ data show variations with the amplitude of 3‰ since the last deglaciation, including high $\delta^{18}O$ values during the BA, the early Holocene, and the late Holocene, and low $\delta^{18}O$ values during the YD and the middle Holocene. The negative shift in $\delta^{18}O$ during the YD is synchronous with Greenland ice-core and central European lake $\delta^{18}O$ records [40], indicating concurrent millennial-scale climate cooling in central North America. The climate cooling during the YD is also supported by *Picea* (spruce) pollen zone that represents cold forest ecosystem. High $\delta^{18}O$ values during the early Holocene indicate higher temperature than the YD. Climate amelioration during the early Holocene is also supported by regional vegetation dominated by *Pinus* (pine) and *Quercus* (oak), characterizing warm forest ecosystem. However, multiple lines of evidence from lithological and paleoecological analyses show that lake level was lower at Crawford Lake during the middle Holocene, likely caused by a dry climate. A 2.4‰ negative shift in carbonate $\delta^{18}O$ during this interval is seemingly at odds with overall warm and dry climate. Enhanced evaporation under dry conditions should have driven a positive shift of carbonate $\delta^{18}O$. Cooling with a magnitude comparable with the YD is unlikely as the forest is mostly stable during this interval. Instead, the negative shift of $\delta^{18}O$ might be caused by changes in atmospheric circulation patterns. Prior to the middle Holocene, the dominant precipitation source was from the Gulf of Mexico carried by warm and moist air mass trajectories (with high $\delta^{18}O$ values). Increasing proportion of Pacific-sourced precipitation carried by cold and dry air mass trajectories (with low $\delta^{18}O$ values) is likely

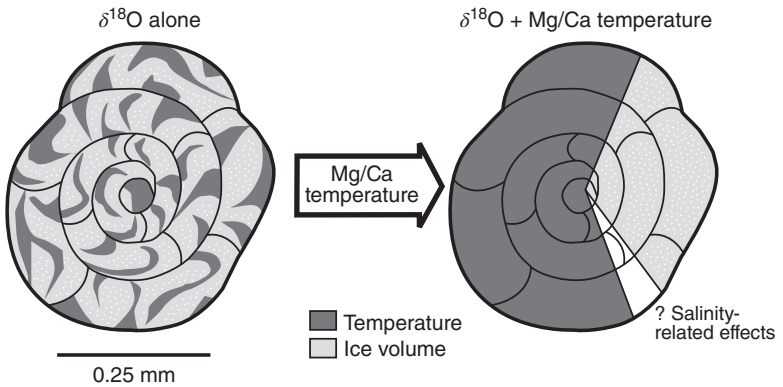

Figure 10 Cartoon illustrates that by including independent paleotemperature estimates from Mg/Ca proxy of deep-sea foraminifera, the mixing signals of ocean temperature and ice volume documented by foraminifera $\delta^{18}O$ data could be isolated (Source: Redrawn from [64]). The shell depicted is benthic foraminifer genus *Oridorsalis* [63].

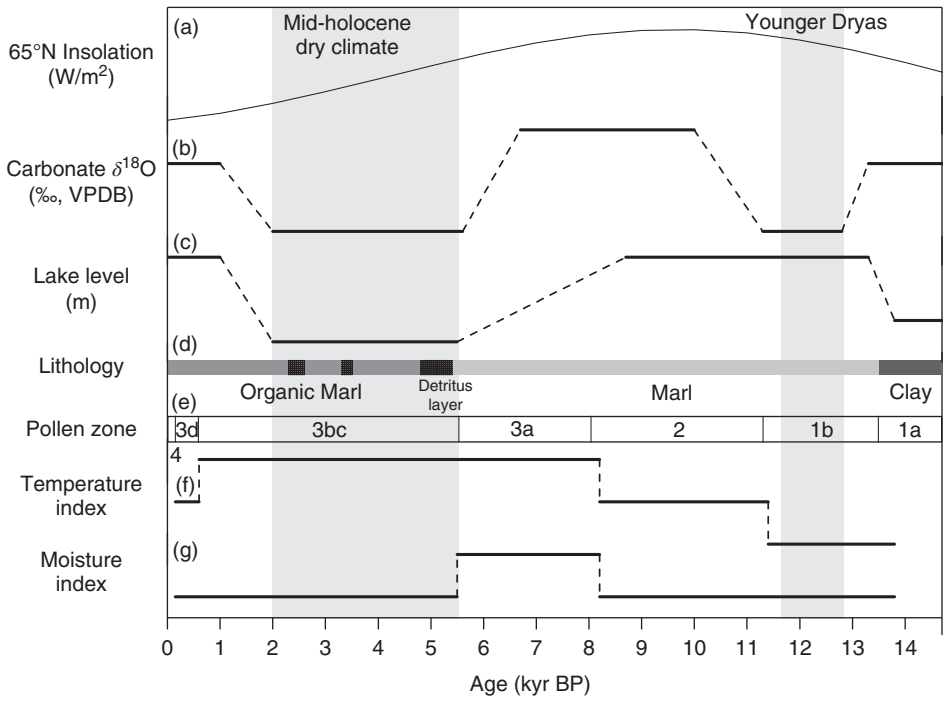

Figure 11 Schematic summary of multi-proxy paleoclimate reconstruction since the last deglaciation from sediment cores of Crawford Lake in southern Ontario, Canada [66, 67]: (a) 65° N summer insolation [21]; (b) lacustrine carbonate $\delta^{18}O$ record; (c) lake-level estimates based on lithology, sediment hiatus and macrofossils; (d) sediment-core lithology; (e) pollen zones including 1a (herb/shrub zone), 1b (*Picea* zone), 2 (*Pinus* zone), 3a (*Tsuga* subzone), 3bcd (*Fagus* subzones) and 4 (*Ambrosia* zone); (f) temperature index and (g) moisture index based on the pollen assemblages. The negative shifts in $\delta^{18}O$ during the YD and the middle Holocene (grey bars) are explained by climate cooling, and changes in atmospheric circulation patterns, respectively.

to explain the negative shift of $\delta^{18}O$ during this interval. Recent studies in central North America further support that different moisture sources have distinct isotopic composition and their proportions varied significantly over time [68]. Overall, the way to interpret isotopic variations in terms of certain factor is not consistent during different intervals, but multi-proxy approach could constrain the isotope-based interpretations.

Further Reading

Bradley, R.S. (2015). *Paleoclimatology: Reconstructing Climates of the Quaternary*, 3e. San Diego, CA, USA: Academic Press.

Hoefs, J. (2008). *Stable Isotope Geochemistry*, 6e. Göttingen, Germany: Springer-Verlag Berlin Heidelberg.

Kendall, C. and McDonnell, J.J. (1998). *Isotope Tracers in Catchment Hydrology*. Amsterdam, Netherlands: Elsevier Science Publisher.

Sharp, Z. (2005). *Principles of Stable Isotope Geochemistry*. Upper Saddle River, NJ, USA: Pearson Prentice Hall.

References

1 Gat, J.R. (2010). *Isotope Hydrology: a Study of the Water Cycle*. London, UK: Imperial College Press.

2 LeGrande, A.N. and Schmidt, G.A. (2006). *Geophys. Res. Lett.* 33: L12604. doi: 10.1029/2006GL026011.

3 Bowen, G.J. and Revenaugh, J. (2003). *Water Resour. Res.* 39: 1299. doi: 10.1029/2003WR002086.

4 Clark, I.D. and Fritz, P. (1997). *Environmental Isotopes in Hydrogeology*. Boca Raton, FL, USA: CRC Press.

5 Dansgaard, W. (1964). *Tellus* 16: 436–468. doi: 10.3402/tellusa.v16i4.8993.

6 Gat, J.R., Mook, W.G., and Meijer, H.A.J. (2001). *Environmental Isotopes in the Hydrological Cycle: Principles and Applications*, UNESCO/IAEA Series, Paris, France, 2 (ed. W.G. Mook), 167–235.

7 Poage, M.A. and Chamberlain, C.P. (2001). *Am. J. Sci.* 301: 1–15. doi: 10.2475/ajs.301.1.1.

8 Craig, H. (1961). *Science* 133: 1702–1703. doi: 10.1126/science.133.3465.1702.

9 Sustainability of Semi-Arid Hydrology and Riparian Areas. http://web.sahra.arizona.edu/programs/isotopes/oxygen.html (accessed 20 October 2017).

10 Mayr, C., Lücke, A., Stichler, W. et al. (2007). *J. Hydrol.* 334: 53–63. doi: 10.1016/j.jhydrol.2006.09.025.

11 Uemura, R., Matsui, Y., Yoshimura, K. et al. (2008). *J. Geophys. Res. Atmos.* 113: D19114. doi: 10.1029/2008JD010209.

12 Pfahl, S. and Sodemann, H. (2014). *Clim. Past* 10: 771–781. doi: 10.5194/cp-10-771-2014.

13 Craig, H. and Gordon, L.I. (1965). *Stable Isotopes in Oceanographic Studies and Paleo-Temperatures* (ed. E. Tongiorgi), 9–130. Pisa, Spoleto, Italy: V. Lishi e F.
14 Gasse, F. (2009). *Encyclopedia of Paleoclimatology and Ancient Environments* (ed. V. Gornitz), 733–738. Dordrecht, Netherlands: Springer.
15 Jouzel, J., Hoffmann, G., Koster, R.D., and Masson, V. (2000). *Quat. Sci. Rev.* 19: 363–379. doi: 10.1016/S0277-3791(99)00069-4.
16 Kim, S.-T. and O'Neil, J.R. (1997). *Geochim. Cosmochim. Acta* 61: 3461–3475. doi: 10.1016/S0016-7037(97)00169-5.
17 Lisiecki, L.E. and Raymo, M.E. (2005). *Paleoceanography* 20: PA1003. doi: 10.1029/2004PA001071.
18 Luthi, D., Le Floch, M., Bereiter, B. et al. (2008). *Nature* 453: 379–382. doi: 10.1038/nature06949.
19 Wang, Y., Cheng, H., Edwards, R.L. et al. (2008). *Nature* 451: 1090–1093. doi: 10.1038/nature06692.
20 Cheng, H., Edwards, R.L., Sinha, A. et al. (2016). *Nature* 534: 640–646. doi: 10.1038/nature18591.
21 Berger, A. and Loutre, M.F. (1991). *Quat. Sci. Rev.* 10: 297–317. doi: 10.1016/0277-3791(91)90033-Q.
22 Zachos, J., Pagani, M., Sloan, L. et al. (2001). *Science* 292: 686–693. doi: 10.1126/science.1059412.
23 Shackleton, N.J., Backman, J., Zimmerman, H.t. et al. (1984). *Nature* 307: 620–623. doi: 10.1038/307620a0.
24 Ruddiman, W.F. (2013). *Earth's Climate: Past and Future*, 3e. New York, NY, USA: W. H. Freeman and Company.
25 Ahn, J. and Brook, E.J. (2008). *Science* 322: 83–85. doi: 10.1126/science.1160832.
26 Stenni, B., Masson-Delmotte, V., Johnsen, S. et al. (2001). *Science* 293: 2074–2077. doi: 10.1126/science.1059702.
27 Steffensen, J.P., Andersen, K.K., Bigler, M. et al. (2008). *Science* 321: 680–684. doi: 10.1126/science.1157707.
28 Guan, J., Liu, Z., Wen, X. et al. (2016). *J. Geophys. Res. Atmos.* 121: 342–354. doi: 10.1002/2016JD024955.
29 N.G.I.C.P. Members (2004). *Nature* 431: 147–151. doi: 10.1038/nature02805.
30 McManus, J.F., Francois, R., Gherardi, J.M. et al. (2004). *Nature* 428: 834–837. doi: 10.1038/nature02494.
31 E.C. Members (2006). *Nature* 444: 195–198. doi: 10.1038/nature05301.
32 Jouzel, J., Masson-Delmotte, V., Cattani, O. et al. (2007). *Science* 317: 793–796. doi: 10.1126/science.1141038.
33 Monnin, E., Indermühle, A., Dällenbach, A. et al. (2001). *Science* 291: 112–114. doi: 10.1126/science.291.5501.112.
34 Leng, M.J. and Marshall, J.D. (2004). *Quat. Sci. Rev.* 23: 811–831. doi: 10.1016/j.quascirev.2003.06.012.
35 Huang, Y., Shuman, B., Wang, Y., and Webb, I.I.I.T. (2002). *Geology* 30: 1103–1106. doi: 10.1130/0091-7613(2002)030<1103:HIROPA>2.0.CO;2.
36 Sachse, D., Billault, I., Bowen, G.J. et al. (2012). *Annu. Rev. Earth Planet. Sci.* 40: 221–249. doi: 10.1146/annurev-earth-042711-105535.
37 Leng, M.J. and Barker, P.A. (2006). *Earth Sci. Rev.* 75: 5–27. doi: 10.1016/j.earscirev.2005.10.001.
38 Mayr, C., Lücke, A., Wagner, S. et al. (2013). *Geology* 41: 831–834. doi: 10.1130/G34335.1.
39 Rozanski, K., Araguás-Araguás, L., and Gonfiantini, R. (1992). *Science* 258: 981–985. doi: 10.1126/science.258.5084.981.
40 von Grafenstein, U., Erlenkeuser, H., Brauer, A. et al. (1999). *Science* 284: 1654–1657. doi: 10.1126/science.284.5420.1654.
41 Tierney, J.E., Russell, J.M., Huang, Y. et al. (2008). *Science* 322: 252–255. doi: 10.1126/science.1160485.
42 Shanahan, T.M., Overpeck, J.T., Anchukaitis, K.J. et al. (2009). *Science* 324: 377–380. doi: 10.1126/science.1166352.
43 Steinman, B.A., Abbott, M.B., Mann, M.E. et al. (2012). *Proc. Natl. Acad. Sci. U.S.A* 109: 11619–11623. doi: 10.1073/pnas.1201083109.
44 Henderson, A.K., Nelson, D.M., Hu, F.S. et al. (2010). *Earth Planet. Sci. Lett.* 300: 205–214. doi: 10.1016/j.epsl.2010.09.024.
45 Lachniet, M.S. (2009). *Quat. Sci. Rev.* 28: 412–432. doi: 10.1016/j.quascirev.2008.10.021.
46 Lachniet, M.S., Denniston, R.F., Asmerom, Y., and Polyak, V.J. (2014). *Nat. Commun.* 5: 3805. doi: 10.1038/ncomms4805.
47 Wang, Y., Cheng, H., Edwards, R.L. et al. (2005). *Science* 308: 854–857. doi: 10.1126/science.1106296.
48 Wang, Y.J., Cheng, H., Edwards, R.L. et al. (2001). *Science* 294: 2345–2348. doi: 10.1126/science.1064618.
49 Yuan, D., Cheng, H., Edwards, R.L. et al. (2004). *Science* 304: 575–578. doi: 10.1126/science.1091220.
50 Orland, I.J., Edwards, R.L., Cheng, H. et al. (2015). *Geology* 43: 555–558. doi: 10.1130/G36612.1.
51 McCarroll, D. and Loader, N.J. (2004). *Quat. Sci. Rev.* 23: 771–801. doi: 10.1016/j.quascirev.2003.06.017.
52 Treydte, K.S., Schleser, G.H., Helle, G. et al. (2006). *Nature* 440: 1179–1182. doi: 10.1038/nature04743.
53 Miller, D.L., Mora, C.I., Grissino-Mayer, H.D. et al. (2006). *Proc. Natl. Acad. Sci. U.S.A* 103: 14294–14297. doi: 10.1073/pnas.0606549103.
54 Cobb, K.M., Charles, C.D., Cheng, H., and Edwards, R.L. (2003). *Nature* 424: 271–276. doi: 10.1038/nature01779.
55 Cobb, K.M., Westphal, N., Sayani, H.R. et al. (2013). *Science* 339: 67–70. doi: 10.1126/science.1228246.

56 Jones, M.C., Wooller, M., and Peteet, D.M. (2014). *Quat. Sci. Rev.* 87: 1–11. doi: 10.1016/j.quascirev.2013.12.025.
57 Daley, T.J., Barber, K.E., Street-Perrott, F.A. et al. (2010). *Quat. Sci. Rev.* 29: 1590–1601. doi: 10.1016/j.quascirev.2009.09.017.
58 Nichols, J., Booth, R.K., Jackson, S.T. et al. (2010). *Geochim. Cosmochim. Acta* 74: 1407–1416. doi: 10.1016/j.gca.2009.11.012.
59 Cerling, T.E. (1984). *Earth Planet. Sci. Lett.* 71: 229–240. doi: 10.1016/0012-821X(84)90089-X.
60 Amundson, R., Chadwick, O., Kendall, C. et al. (1996). *Geology* 24: 23–26. doi: 10.1130/0091-7613(1996)024<0023:IEFSIA>2.3.CO;2.
61 Quade, J., Garzione, C., and Eiler, J. (2007). *Rev. Mineral. Geochem.* 66: 53–87. doi: 10.2138/rmg.2007.66.3.
62 Ghosh, P., Garzione, C.N., and Eiler, J.M. (2006). *Science* 311: 511–515. doi: 10.1126/science.1119365.
63 Lear, C.H., Elderfield, H., and Wilson, P.A. (2000). *Science* 287: 269–272. doi: 10.1126/science.287.5451.269.
64 Dwyer, G.S. (2000). *Science* 287: 246–247. doi: 10.1126/science.287.5451.246.
65 Birks, H.H. and Birks, H.J.B. (2006). *Veg. Hist. Archaeobot.* 15: 235–251. doi: 10.1007/s00334-006-0066-6.
66 Yu, Z., McAndrews, J.H., and Eicher, U. (1997). *Geology* 25: 251–254. doi: 10.1130/0091-7613(1997)025<0251:MHDCCB>2.3.CO;2.
67 Yu, Z. and Eicher, U. (1998). *Science* 282: 2235–2238. doi: 10.1126/science.282.5397.2235.
68 Bird, B.W., Wilson, J.J., Gilhooly, W.P. III et al. (2017). *Sci. Rep.* 7: 41628. doi: 10.1038/srep41628.